

Seasonal Reversal of the Near-Surface Chlorophyll Response to the Presence of Mesoscale Eddies in the South Pacific Subtropical Countercurrent

Seth Travis¹ and Bo Qiu

Department of Oceanography, University of Hawai'i at Mānoa, Honolulu, HI, USA

Key Points:

- Chlorophyll response to eddies in the STCC is found to be highly spatially and seasonally variable
- Western STCC patterns are inferred to seasonally reverse from nutrient to light limitation
- Additional metrics are developed to globally identify other regions in which this seasonal reversal pattern may exist

Correspondence to:S. Travis,
stravis3@hawaii.edu**Citation:**

Travis, S., & Qiu, B. (2020). Seasonal reversal of the near-surface chlorophyll response to the presence of mesoscale eddies in the South Pacific Subtropical Countercurrent. *Journal of Geophysical Research: Oceans*, 125, e2019JC015752. <https://doi.org/10.1029/2019JC015752>

Received 9 OCT 2019

Accepted 3 MAR 2020

Accepted article online 10 MAR 2020

Abstract Mesoscale eddies have been shown to have significant effects on biogeochemical cycles, as observed in local levels of near-surface chlorophyll. There are many regional differences in the expected response of near-surface chlorophyll to the presence of eddies, caused by differences in the driving mechanisms. However, in many high eddy activity areas, previous studies found low correlation and an inconsistent chlorophyll anomaly response to the presence of eddies. One such area is in the South Pacific Subtropical Countercurrent. Using GlobColour ocean color data and Aviso altimetry data, an investigation of the area found that a seasonal reversal occurs in the character of the chlorophyll anomaly within eddies (reversal from positive to negative and vice versa). The cause of this reversal is inferred to be a seasonally changing limiting factor within the region. Argo float profiles colocated inside and outside of eddies are used to show the coincidence of chlorophyll anomalies with seasonally changing mixed layer depths and the ability of the eddies to access deep nutrient pools. Observations of other mechanisms, such as eddy stirring or eddy-Ekman pumping, are found to be seasonally less important than the mixed layer depth change-induced nutrient flux. Additionally, metrics are developed to globally identify oceanic regions in which such seasonal reversals in chlorophyll anomalies could occur.

Plain Language Summary Mesoscale ocean eddies are large swirling masses of water, on the scale of 100 km in diameter, and have anomalous water properties. Eddies have been found to alter phytoplankton concentrations in their waters. In the low-nutrient waters of the western South Pacific gyre, cyclonic eddies (eddies which spin clockwise) are found to have lower chlorophyll concentrations while anticyclonic eddies (eddies which spin counterclockwise) have higher chlorophyll concentrations. However, in the western branch of the South Pacific Subtropical Countercurrent (STCC), seasonal changes in mixed layer depth and light and nutrient availability cause a seasonal reversal in the expected chlorophyll anomaly in eddies (reversal from negative to positive and vice versa). This research provides a study of the observed chlorophyll anomaly signals in eddies across the STCC and of the various forcings and limiting factors which impact these anomalies. Additionally, preliminary work is done to identify additional areas, globally, in which these seasonal reversals occur.

1. Introduction

Primary production in the ocean can be strongly affected by mesoscale eddies (Chelton et al., 2011; Gaube et al., 2014; Klein & Lapeyre, 2009; McGillicuddy, 2016), which can trap and transport waters, advect water properties and nutrients across gradients, and generate vertical movements of waters and nutrients. Implications for the local influence of eddies on biological activity are diverse. Local primary production can effect net carbon flux to the deep ocean (Guidi et al., 2012), and increased productivity in a region can increase biological abundance at higher trophic levels (Godø et al., 2012; Lavelle & Mohn, 2010; Morato et al., 2009). Eddies have been shown to trap planktonic communities over multiple generations (Condie & Condie, 2016), while Shulzitski et al. (2016) found that larval coral fish communities entrained within some eddies have higher survivability to settlement on coral reefs. Cyclonic eddies have even been shown to be a preferred foraging habitat for Kerguelen elephant seals in the Polar Frontal Zone of the Southern Ocean (Bailleul et al., 2010). Because of this wide range of possible physical-biological interactions, an understanding of the driving mechanisms and the subsequent biological responses is crucial.

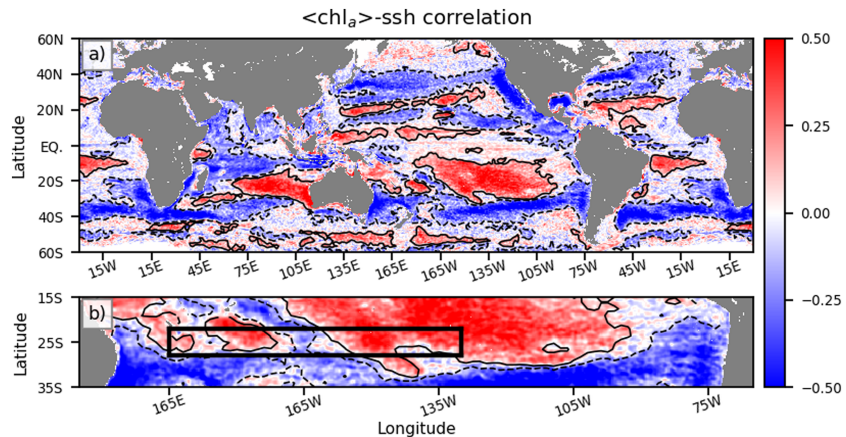


Figure 1. (a) Global map of $\langle \text{chl}_a \rangle\text{-ssh}$ anomaly cross correlation. (b) South Pacific map of $\langle \text{chl}_a \rangle\text{-ssh}$ anomaly cross correlation, with the STCC region of study indicated by the black box from 22°S to 28°S and 165°E to 130°W. In both maps, cross correlation is taken between spatially high-passed SSH anomalies and chl_a anomalies. The cross correlation has been spatially smoothed with a second-order Lanczos filter with a 1° half-width window. The solid black contours indicate areas of significant positive cross correlation (>0.1), and the dashed black contours indicate areas of significant negative cross correlation (<-0.1). Correlation significance is calculated at the 95% significance level, following von Storch and Zwiers (1999), using the formula $q_t(\pm 0.025; n - 2) / \sqrt{n}$, where $q_t(\pm 0.025; n)$ is the 2.5 percentage point of the Student's t distribution with $n - 2$ degrees of freedom, and n is estimated as the number of days of data.

A useful proxy of phytoplankton biomass is the near-surface chlorophyll signal, for which we have an increasingly robust data record through ocean color satellite programs such as SeaWiFS and MODIS/Aqua, among others. The mean near-surface chlorophyll concentrations can vary by orders of magnitude and are not necessarily associated with areas of strong eddy activity. However, as has been shown in other regions, eddies can have a significant effect on the near-surface chlorophyll levels (Chelton et al., 2011; Dufois et al., 2014; Gaube et al., 2013, 2014, He, Zhan, Cai, & Li 2016; Huang & Xu, 2018). The cross correlation between spatially high-passed chlorophyll anomalies and sea surface height anomalies, recreated as following Gaube et al. (2014) to isolate mesoscale features, is shown in Figure 1. There is large spatial variability in this cross correlation, indicating significant variation in the near-surface chlorophyll response to the presence of eddies. One such area with an inconsistent chlorophyll anomaly to sea surface height anomaly correlation is in the South Pacific Subtropical Countercurrent (STCC) (see Figure 1b). This is an area of heightened eddy activity with a relatively weak mean current (approximately $3\text{--}5 \text{ cm s}^{-1}$), and the pinching off of meanders has not been observed to be a significant feature. The current is associated with baroclinic instabilities (Qiu et al., 2008; Rieck et al., 2018; Travis & Qiu, 2017) and spans a transition into highly oligotrophic waters as moving downcurrent from west to east. This study explores the possible driving mechanisms in the region which could cause the inconsistent response. Known driving mechanisms include trapping of surface waters and nutrients during eddy formation to sustain chlorophyll anomalies, stirring of surface waters and chlorophyll gradients, mixed layer depth anomalies affecting the availability of access to deep nutrient pools, and upwelling/downwelling generated during eddy formation, through eddy-Ekman pumping or by submesoscale frontal processes (Chelton et al., 2011; Dufois et al., 2014; Gaube et al., 2013; He, Zhan, Cai, & Li 2016; Martin & Richards, 2001; McGillicuddy, 2016; Zhang et al., 2014, 2019).

When eddies form, they can trap waters of a particular temperature and/or salinity (Dong et al., 2014; Dufour et al., 2015) as well as local phytoplankton and nutrients. As the eddies move throughout the ocean, they can carry these signatures with them. This mechanism is particularly important during the start of the eddy life cycle, as any nutrients can be quickly consumed to support biological activity already present in the eddy. Eddy stirring is important at gradients of chlorophyll, where the largely horizontal eddy currents skew the surface gradients, creating a dipole of positive and negative chlorophyll signals based upon the strength of the gradient, the orientation of the gradient, and the strength of the eddy. These horizontal mechanisms primarily create chlorophyll anomalies through advection of chlorophyll and do not necessarily involve any change in levels of primary production in the region (Chelton et al., 2011; McGillicuddy, 2016)

Cyclonic/anticyclonic eddies generate upwelling/downwelling during their intensification periods, the initial growth and development period of eddies. This is typically on the order of 1 m day^{-1} (Gaube et al., 2015). Eddy-induced Ekman pumping is caused by the curl of surface wind stress due to the relative motions of the surface currents and surface winds (Gaube et al., 2015; Martin & Richards, 2001). Locally, this can be larger than the Ekman pumping caused by the surface stress derived only from the curl of the surface winds, as the eddy-induced wind stress curl occurs over length scales of hundreds of kilometers, much smaller than the regional Ekman pumping. Relative to the eddy pumping during the spin-up of the eddy, this is an order of magnitude smaller ($\sim 10 \text{ cm day}^{-1}$). Gaube et al. (2015) explored the regional strength of eddy-induced Ekman pumping, including an area to the northeast of the South Pacific STCC region, and found a typical eddy-Ekman-induced pumping velocity is 8 cm day^{-1} . This mechanism would be present throughout the life cycle of the eddy and, in the case of eddy-Ekman-induced upwelling in anticyclones, can provide a continuous source of deep nutrients to the euphotic zone. Lastly, frontal instabilities have been shown to create strong vertical velocities at the submesoscale (Klein & Lapeyre, 2009; Zhang et al., 2019); however, this mechanism will be outside of the purview of this work.

Mixed layer depth anomalies are also expected to alter the surface expression of chlorophyll concentrations. It has been observed that anticyclones typically have deeper mixed layers than cyclones (Dufois et al., 2014; Gaube et al., 2019; He, Zhan, Cai, & Li 2016) due to the relative isopycnal displacement of the two types of eddies. As described in McGillicuddy (2016), the expected character of the phytoplankton response to mixed layer depth anomalies is dependent on whether light or nutrients limit phytoplankton growth. In highly oligotrophic, low-nutrient regions, deeper mixed layers are able to access a deep pool of nutrients which would otherwise be unavailable in the surface waters. In these cases, the deeper mixed layers of anticyclones can spur higher chlorophyll levels than cyclones, as they are able to access a larger nutrient pool. Conversely, in a highly productive, high-nutrient region, there are often sufficient nutrients, and it is the lack of sufficient light penetration which prevents further production. In this case, the deeper mixed layers can cause mixing to occur deeper than the euphotic layer. When this happens, phytoplankton in the mixed layer receive lower average ambient light, thus decreasing productivity. In these cases, the deep mixed layers of anticyclones would lead to lower chlorophyll levels than cyclones.

Large portions of the oceanic basins are in areas of low mean chlorophyll, which often have nutriclines too deep to have injection of nutrients into the mixed layer (McClain et al., 2004). Mignot et al. (2014) examined the seasonality of these oligotrophic areas, finding that the seasonal depth of the mixed layer is important in determining whether changes in near-surface chlorophyll are caused by new production or changes in intracellular pigmentation due to photoacclimation. Similarly, Dufois et al. (2016) found that anticyclonic eddies have elevated chlorophyll levels in subtropical gyres due to deep winter mixing. In the South Pacific, the oligotrophic region of the gyre is found to have very low nutrient levels and an exceptionally deep nutricline (Bender & Jonsson, 2016; Dufois et al., 2016). He, Zhan, Cai, and Li (2016), as well as others (Chelton et al., 2011; Dufois et al., 2014), found a connection between the chlorophyll response to the presence of eddies and the relative depths of the mixed layer and the nutricline. A deep nutricline could prevent eddies from having a strong effect of local productivity. However, in regions of transition between highly oligotrophic waters with a particularly deep nutricline and more productive waters, typically closer to coastal areas, the seasonally varying mixed layer depth could cause intermittent access to this deep nutrient pool.

The wide range of forcing mechanisms and the varied responses to these forcings, as well as the seasonally varying environment in which the eddies are situated, create a complex system. Careful consideration of the relative strengths of each of these forcings is required. It is hypothesized that the eddying STCC region crosses a transition region from a modestly productive region to one of ultralow-nutrient availability (Bender & Jonsson, 2016) and that within this transition seasonally changing access to deep nutrient pools can result in a seasonally alternating character of response of near-surface chlorophyll in eddies. A seasonal analysis is needed to fully quantify the effect that eddies have on biological signals in the region. Using a combination of data of near-surface chlorophyll, sea surface height, and eddy tracks, seasonal patterns of chlorophyll anomalies within eddies can be observed. Additional data, such as light availability, mixed layer depths within eddies, nutrient availability, and wind forcing, can be used to determine the dominant drivers of the chlorophyll anomalies and the subsequent limiting factors.

2. Data and Methods

2.1. Data Sets

An analysis of the regional near-surface chlorophyll response to mesoscale eddies draws from a large number of data sources. These include the GlobColour merged satellite ocean color product, Aviso satellite altimetry data of sea surface height, eddy tracks as provided from the Aviso eddy atlas, Argo float profiles of temperature and salinity, and the Argo float profile mixed layer depth product from Holte et al. (2017). For climatological nutrient data, the World Ocean Atlas 2018 was used (Garcia et al., 2019). Lastly, wind stress data was taken from QuikSCAT V3. Each of these data sets will be used to construct eddy-centric seasonal cycles of the relevant parameters. For anomalies of near-surface chlorophyll, sea surface height, geostrophic velocities, and wind stress, monthly composites can be made to illustrate spatial patterns of these parameters within a “typical” eddy. The analysis period runs from January 2004 to December 2017, with the exception of the wind stress data, for which the analysis will run from January 2000 to December 2008. The period of January 2004 to December 2017 was chosen, as there is robust data coverage in ocean color, satellite altimetry data, and Argo float profiles. The wind data period is chosen to provide maximum observational time coverage in order to construct seasonal patterns of eddy-Ekman pumping.

The Aviso $0.25^\circ \times 0.25^\circ$ gridded daily satellite product of absolute dynamic topography, as processed by CNES/CLS, is used for sea surface height (SSH). Geostrophic velocities are also available and will be used. The data were analyzed from January 2004 to December 2017. A mesoscale eddy trajectory atlas is processed and generated by CNES/CLS. The eddy trajectories are generated following the same method for eddy identification and tracking as developed by Schlax and Chelton (2016). From this atlas, eddy centers and radii were used to approximate the size of the eddies, which can then be used to collocate the corresponding chlorophyll, SSH, and wind stress anomalies within the area of the eddies.

Wind stress data are from a gridded product of daily data with $0.25^\circ \times 0.25^\circ$ spatial resolution, as produced by Ifremer/CERSAT. The data used in producing the gridded product are taken from QuikSCAT V3 data, a reprocessing of QuikSCAT scatterometer wind retrievals. The wind data are produced for the time period of October 1999 to November 2009. For the purposes of this analysis, data from January 2000 to December 2008 are used.

Argo floats are used to examine subsurface characteristics—primarily, they are used to examine mixed layer depths and isopycnal displacements. Argo profiles are accessed from U.S. Global Ocean Data Assimilation Experiment (USGODAE) (<https://www.usgodae.org/argo/argo.html>). Mixed layer depths for individual Argo profiles are taken from the Argo profile mixed layer depth product (Holte et al., 2017).

Nutrient information is taken from climatological nitrate data for the World Ocean Atlas 2018 (Garcia et al., 2019). Climatological monthly means of nitrate are given on $1^\circ \times 1^\circ$ spatial resolution at standard depth levels (47 depth levels in the upper 1,000 m). For the purposes of this analysis, the nitracline shall be defined as the depth where NO_3^- exceeds $1 \mu\text{mol kg}^{-1}$.

The GlobColour ocean color data set is a merged product of the various ocean color sensor platforms in use during the operational periods, such as SeaWiFS (Sea-Viewing Wide Field of View Sensor), MERIS (Medium Resolution Imaging Spectrometer), MODIS (Moderate Resolution Imaging Spectrometer) Aqua, VIIRS (Visible Infrared Imaging Radiometer Suite), and OLCI-A (Ocean Land Color Instrument), giving the advantage of improved temporal and spatial coverage. The $0.25^\circ \times 0.25^\circ$ gridded product of daily data was chosen. For the purposes of this study, the analysis is restricted to the period of January 2004 to December 2017, as this provides spatial and temporal resolution consistency with the SSH data set. From this GlobColour product, the following data are accessed: (a) near-surface chlorophyll-*a* (chl_a) merged using the Garver-Siegel-Maritorena (GSM) (Maritorena et al., 2002) method for type 1 waters; (b) diffuse attenuation coefficient of downwelling irradiance at 490 nm ($k_{d(490)}$), which can be used as a measure of turbidity, while the inverse of the coefficient gives a measure of how deep the satellite is able to “see”; and (c) photosynthetically available radiation (PAR) between 400 and 700 nm, which is a measure of how much solar energy reaches the ocean and is available for photosynthesis. The GSM method is a semianalytic technique for calculating and merging data from multiple sensors and was tuned using chlorophyll data in the range of $0.02\text{--}10 \text{ mg m}^{-3}$. It should be noted that while the method has no theoretical limits, the range of values observed in the regional seasonal background chlorophyll levels approaches the bottom limit of this range. A combination of these parameters is used to test for changes in light penetration depth and any chlorophyll

changes due to photoacclimation, which is the adjustment of intracellular pigmentation compensating for changing ambient light levels (Behrenfeld et al., 2005).

2.2. Methods

While the GlobColour product provides improved spatial and temporal coverage by drawing upon the data from multiple sensors, the data can still have gaps due to lack of coverage for a specific day or from cloud coverage preventing observation of an area. To help fill the gaps, a spatiotemporal smoothing of the data is performed. First, the chlorophyll data are \log_{10} transformed to account for the skewed distribution of chlorophyll measurements (Campbell, 1995). Following this, a three-dimensional convolution with a second-order Lanczos window is then applied to the data to help interpolate between points. The Lanczos window has a 7-day temporal half width and a 0.5° half width in the latitudinal and longitudinal directions, respectively. Additionally, the interpolated data point is only used if the summed weight given to the nearby observations exceeds the maximum weighted point in the window, that is, the point at which the interpolation occurs; if the summed weight of the points for which data are available is not larger than the maximum weight, then the point is left as a missing gap. This is done to ensure that any interpolation is sufficiently robust and not done by an interpolation from the points only at the edge of the window.

After filling the data gaps, additional processing of the chlorophyll data is done to attempt to remove small-scale, high-frequency signals which are not associated with mesoscale dynamics. This can include signals associated with intermittent bloom events (He, Zhan, Cai, & Li 2016) or events associated with filament structures along submesoscale instability fronts (Zhang et al., 2019). First, the data are temporally smoothed using a second-order Lanczos filter with a 30-day half width. Next, a second-order Lanczos filter with a 1° half width is applied in the longitudinal and latitudinal directions.

The chlorophyll data are log transformed back to linear concentrations (chl_a), and a spatial high-pass Lanczos filter with a 6° half width is applied to isolate the mesoscale features (chl'_a), removing larger basin-scale signals ($\overline{chl_a}$), such as seasonal background levels.

$$chl'_a = chl_a - \overline{chl_a} \quad (1)$$

The residual from this filtering, being the low-pass Lanczos filtered data, is retained to give a measure of the background chlorophyll state, which permits basin-wide chlorophyll changes such as a seasonal cycle. These methods follow similar work by others observing mesoscale features (Chelton et al., 2011; Gaube et al., 2014; He, Zhan, Cai, & Li, 2016; He, Zhan, Cai, & Zha, 2016). These filtering processes are also applied to $k_{d(490)}$, while the last step of spatial high-pass filtering is also applied to SSH, geostrophic velocities, and wind stress data for consistency. The filtering process allows the retention of the chlorophyll anomalies (chl'_a), the background, seasonally varying chlorophyll ($\overline{chl_a}$), and the normalized chlorophyll anomalies ($\langle chl_a \rangle$), which is the ratio of the chlorophyll anomaly to the background chlorophyll.

$$\langle chl_a \rangle = \frac{chl'_a}{\overline{chl_a}} \quad (2)$$

Figure 1a shows the global patterns of the cross correlation between near-surface chlorophyll-a anomalies and sea surface height anomalies, recreated following Gaube et al. (2014). Figure 1b provides a closer look at the patterns within the South Pacific, with the eddying region of the South Pacific STCC highlighted within the black box, which runs from 165°E to 130°W and $22\text{--}28^\circ\text{S}$. In the STCC, there is a predominantly positive $\langle chl_a \rangle$ -ssh correlation in the eastern half of the box while the western half of the box has no clear positive or negative pattern. For this reason, the analysis in this paper will divide the STCC region into an eastern and western analysis region. The western region extends from 165°E to 170°W , and the eastern half extends within $160\text{--}130^\circ\text{W}$. To examine the seasonal and regional differences in chlorophyll response to eddies, the following analyses are performed:

1. A Hovmueller diagram of $\langle chl_a \rangle$ across a latitudinal band ($22\text{--}28^\circ\text{S}$) is created to reconstruct a seasonal cycle while also examining some spatial variability. This is done separately for cyclones and anticyclones. To do so, the average chlorophyll anomaly within all cyclones (anticyclones) within a 5° longitude box for a given month are binned to find the average anomaly.

Table 1

Overview of Eddy Statistics for Each Region in the South Pacific Subtropical Countercurrent for the Time Period of January 2004 to December 2017

Parameters	West (165°W to 165°E)		East (160–130°E)	
	Anticyclones	Cyclones	Anticyclones	Cyclones
Average N per month	2,419 ± 159	2,549 ± 156	3,279 ± 249	3,337 ± 123
Average N^* per month	102 ± 7	111 ± 7	132 ± 11	137 ± 7
Length (km)	100 ± 32	96 ± 32	96 ± 31	93 ± 30
Axial speed (cm s^{-1})	24.3 ± 7.6	25.3 ± 7.6	16.7 ± 5.2	17.6 ± 5.4
Max $\langle \text{chl}_a \rangle$	6.10 ± 2.66	3.34 ± 1.50	5.90 ± 0.94	−0.64 ± 1.48
Min $\langle \text{chl}_a \rangle$	−3.14 ± 1.30	−6.17 ± 1.67	0.98 ± 1.54	−5.29 ± 0.78
Max chl'_a ($10^{-2} \text{ mg m}^{-3}$)	0.55 ± 0.24	0.53 ± 0.24	0.31 ± 0.05	−0.30 ± 0.03
Min chl'_a ($10^{-2} \text{ mg m}^{-3}$)	−0.38 ± 0.15	−0.53 ± 0.14	0.03 ± 0.05	−0.02 ± 0.04
Max $\langle \text{chl}_a \rangle$ month	February	August	August	December
Min $\langle \text{chl}_a \rangle$ month	September	March	December	July
Min $\overline{\text{chl}}_a$ ($10^{-2} \text{ mg m}^{-3}$)		7.8		2.6
Max $\overline{\text{chl}}_a$ ($10^{-2} \text{ mg m}^{-3}$)		16.3		6.2

Note. N is the total number of eddy realizations during a given month. N^* is the number of individual eddies during a given month. Confidence intervals (\pm ranges) are 1 standard deviation for N , N^* . Length, and Axial speed. Confidence intervals for $\langle \text{chl}_a \rangle$ and chl'_a are 95% intervals, as calculated using the Student's t distribution.

2. Composite averages of the $\langle \text{chl}_a \rangle$, ssh, geostrophic velocities, and wind stress fields can be made. The composites are made by using the eddy track atlas to identify the location of the eddy center and the size of the eddy (eddy radius). For each instance of an eddy, the distance from the eddy center is normalized by the eddy radius, the x - y coordinate axes are aligned perpendicular to the strongest local background chlorophyll gradient, and data within ± 2 eddy radii are used to create the composites (i.e., data from ± 2 eddy radii in the x and y directions). In the normalization, 0 is the eddy center, and ± 1 is the edge of the eddy. This method allows for the construction of eddy composites from eddies of various sizes and is frequently used in studies of eddy anomalies (Chelton et al., 2011; Dawson et al., 2018; Dufois et al., 2016, 2017; Frenger et al., 2018; Gaube et al., 2013, 2014, 2015; He, Zhan, Cai, & Li 2016; Song et al., 2018). Table 1 provides statistical information on the eddies used in creating the composites. For consistency, the spatial chlorophyll gradient ($\nabla \langle \text{chl}_a \rangle$) is calculated, and the data are rotated such that the maximum chlorophyll gradient occurring within an eddy decreases in the positive y direction (i.e., the chlorophyll decreases from a maximum at the bottom of the composite to a minimum at the top of the composite). Composites are made onto a ± 2 eddy radius window with one-eighth eddy radius step size for grid resolution. Additional composites are made of SSH anomalies, geostrophic velocities, and wind stress curl anomalies. These composites are made over the same spatial region as the chlorophyll composites and are subjected to the same rotation. In the case of the wind stress curl composites, the data are rotated such that the large-scale wind field is in the positive x direction (left to right). Using the background chlorophyll data and the Aviso geostrophic velocity data, composites are made of the material derivative of chlorophyll ($D(\text{chl}_a)/Dt$). The material derivative is the sum of the local time rate of change and the advection of the signal gradient.

$$\frac{D(\text{chl}_a)}{Dt} = \frac{\partial}{\partial t} (\text{chl}_a) + \mathbf{u} \cdot \nabla (\text{chl}_a) \quad (3)$$

In this equation, the time derivative is the local rate of change. \mathbf{u} is the geostrophic velocity vector and $\nabla(\text{chl}_a)$ is the chlorophyll gradient, with $\mathbf{u} \cdot \nabla(\text{chl}_a)$ representing the advection of the chlorophyll gradient. The advection of the chlorophyll gradient by geostrophic velocity includes the advection of both the background chlorophyll ($\overline{\text{chl}}_a$) and the chlorophyll anomaly (chl'_a). The time derivative of chlorophyll is calculated using a central differencing scheme in time. The chlorophyll gradients are calculated using forward differencing in space. The material derivative can then be normalized by the background chlorophyll gradient to create $D(\text{chl}_a)/Dt$. Composites of $D(\text{chl}_a)/Dt$ are constructed to explore the effect of the advection of background chlorophyll by eddies on the observed chlorophyll anomalies.

From the composites of chlorophyll anomalies and the chlorophyll material derivative, the monopole/dipole structure is found. Following He, Zhan, Cai, and Li (2016), the monopole structure is found by calculating the radially averaged signal from each composite. The dipole structure is taken as the residual after the monopole structure is removed from the original composite.

The eddy composites are averaged by month. In connection with the Hovmueller diagrams, these can illustrate how the structure of the chlorophyll anomaly response changes by region, by season, and by eddy type.

3. Eddy composites are separated into their monopole and dipole structures for the $\langle \text{chl}_a \rangle$ and $D(\text{chl}_a)/Dt$. Monthly composites are combined into 3-month quarterly averages, with the quarterly periods centered on the month of the maximum of amplitude in the seasonal reversal. For example, if the yearly average cyclonic $\langle \text{chl}_a \rangle$ for a region is positive, and the region experiences a large negative value (i.e., the maximum magnitude of the seasonal reversal) in July, then the quartile will be centered in July, with all subsequent quartiles conforming as necessary.
4. Eddy composites of eddy-Ekman pumping are created for the available time period of the data. The composites are constructed by quarter, as found for the monopole/dipole structures, and by eddy type. Eddy-Ekman pumping can be decomposed into surface current-induced Ekman pumping, vorticity gradient-induced Ekman pumping, and a planetary gradient-induced Ekman pumping (Gaubert et al., 2015). However, for the purpose of this paper, only the surface current-induced Ekman pumping is considered, as it typically is of the largest magnitude:

$$w_{ek} = \frac{\nabla \times \bar{\tau}}{\rho(f + \zeta)} \quad (4)$$

where $\bar{\tau}$ is the surface wind stress, ρ is the reference seawater density of $1,025 \text{ kg m}^{-3}$, f is the Coriolis parameter at the eddy center, and ζ is the local vorticity within the eddy. In an idealized scenario of constant wind forcing over an eddy, the surface current-induced Ekman pumping would have a monopole structure with a maximum magnitude at the eddy center (Martin & Richards, 2001).

5. Within each region, the seasonal cycle of nitrate availability as distributed with depth is found. The nitracline depth, being defined as the depth where nitrate exceeds $1 \mu\text{mol L}^{-1}$ ($\text{NO}_3^- > 1 \mu\text{mol kg}^{-1}$), is calculated for each month. Additionally, this cycle is explored in relation to monthly values of mixed layer depth, the euphotic layer depth (z_{eu}), and the averaged nitrate anomalies within mixed layers of eddies. Mixed layer nitrate concentrations are calculated by determining a monthly averaged mixed layer depth for anticyclones, cyclones, and outside of eddies from colocated Argo profiles, using the Argo MLD database (Holte et al., 2017). This mixed layer depth is then used with the WOA18 nitrate climatology to calculate the mixed layer depth nitrate concentration in anticyclones, cyclones, and outside of eddies for any given month.
6. Regionally averaged seasonal changes are examined for background chlorophyll, chlorophyll anomalies, and photosynthetically available radiation within the mixed layer (PAR_{ML}). Following Morel et al. (2010), PAR_{ML} is calculated as

$$\text{PAR}_{ML} = \frac{1}{MLD} \int_{MLD}^0 \text{PAR}(0) \exp(-k_{d(PAR)} z) \delta z \quad (5)$$

where PAR_{ML} is related to $k_{d(490)}$ by the following equation, following Morel et al. (2007):

$$k_{d(PAR)} = 0.0665 + 0.874k_{d(490)} - 0.00121k_{d(490)}^{-1} \quad (6)$$

Within these equations, $k_{d(490)}$ is the diffuse attenuation coefficient at 490 nm, $\text{PAR}(0)$ is the photosynthetically available radiation at the surface of the ocean, and MLD is the mixed layer depth averaged regionally and within eddies. To calculate MLD, the Argo profile mixed layer depth product (Holte et al., 2017) is used. Annual cycles of MLD for the western and eastern regions are constructed for inside and outside of eddies, and these MLD values are used in equation (5) according to each location's respective case (in cyclones, in anticyclones, or not in an eddy).

A photoacclimation response would show that chl_a has an inverse response to PAR_{ML} . As ambient light levels increase in the summer, phytoplankton are able to respond more efficiently, and require less chlorophyll to sustain photosynthesis. Additionally, shallow summer mixed layers would constrain waters closer to the surface, where ambient light levels are the highest. Conversely, the low ambient light in the winter in combination with deep mixed layers mean that there is less PAR available to phytoplankton. In this case, phytoplankton may need to produce more chlorophyll to meet their photosynthetic demands.

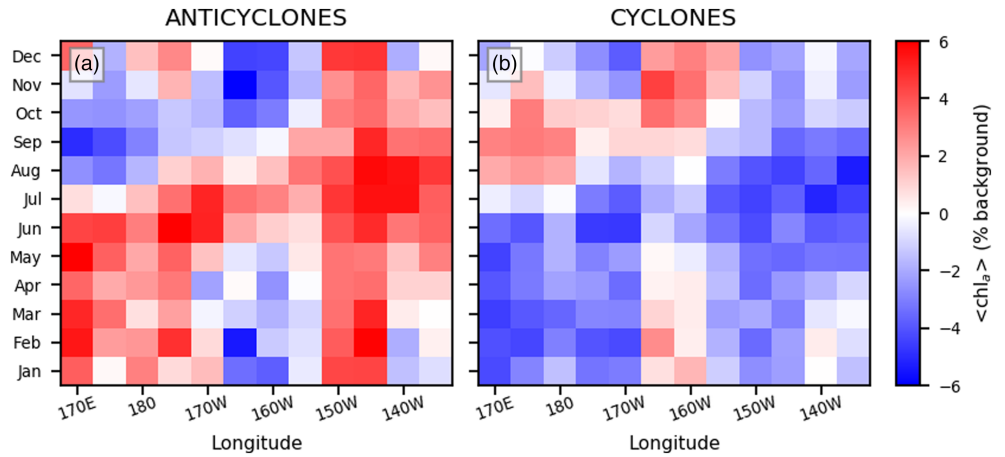


Figure 2. Hovmueller $x-t$ diagram of normalized chlorophyll anomalies ($\langle \text{chl}_a \rangle$) by month. The $x-t$ diagram is averaged between 22°S and 28°S , binned into 5° longitude boxes from 165°E to 130°W . This region is the boxed area seen in Figure 1b. (a) Anticyclones and (b) cyclones.

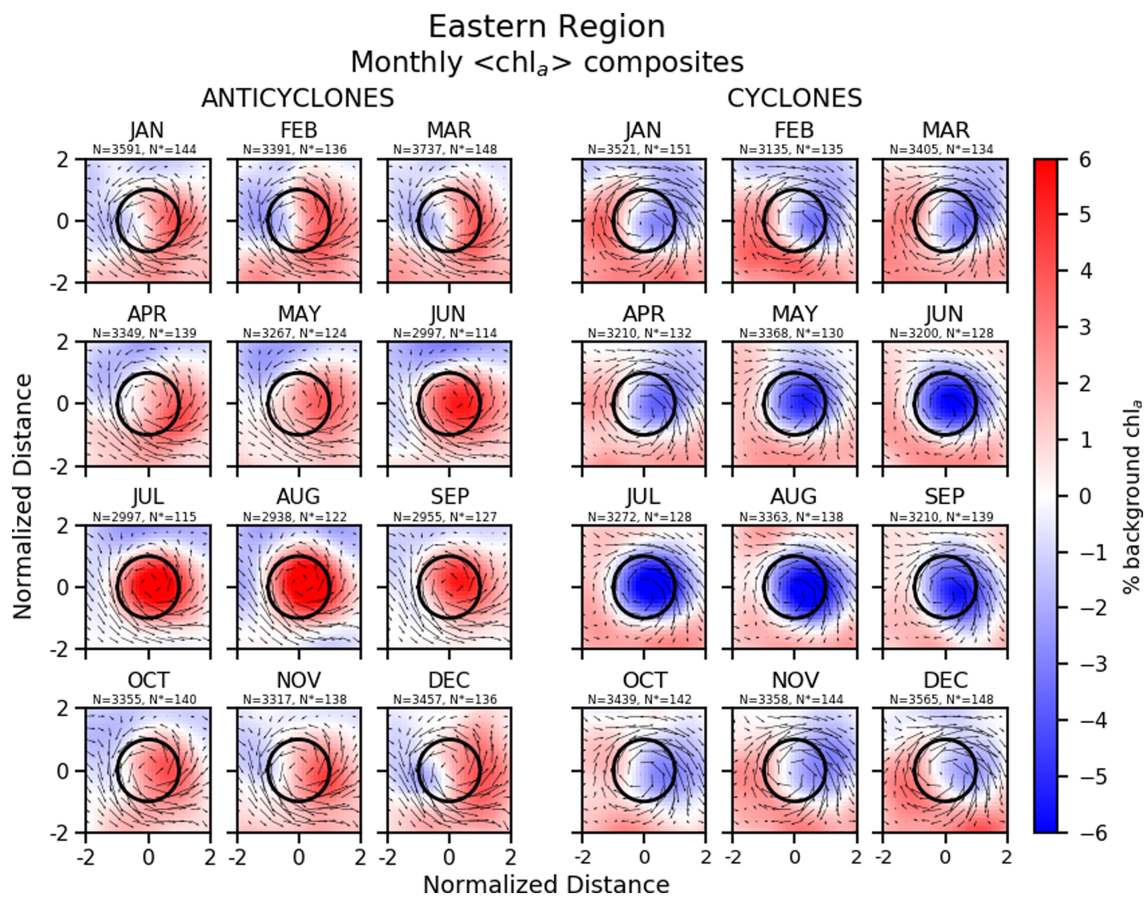


Figure 3. Composites of normalized chlorophyll anomalies in eddies in the eastern South Pacific STCC ($160\text{--}130^\circ\text{W}$) by month, as a percent of the background chlorophyll level. Anticyclones are shown by month in the left half of the figure, while cyclones are shown by month in the right half of the figure. The black circle indicates one eddy radius from the center. The arrows are calculated geostrophic velocity vectors, as calculated from sea surface height anomalies. The color bar indicates the normalized chlorophyll anomaly, given as a percent of the large-scale, background chlorophyll signal. Above each composite, the number of daily eddy composites used for each monthly average is given as N , while the number of individual eddies, which persist throughout the month, is given as N^* . For the purposes of conservative efforts in estimating confidence intervals, seen in Figure 4, N^* is used in an estimate of the number of degrees of freedom. For statistical characteristics of the eddies used in composites, refer to Table 1.

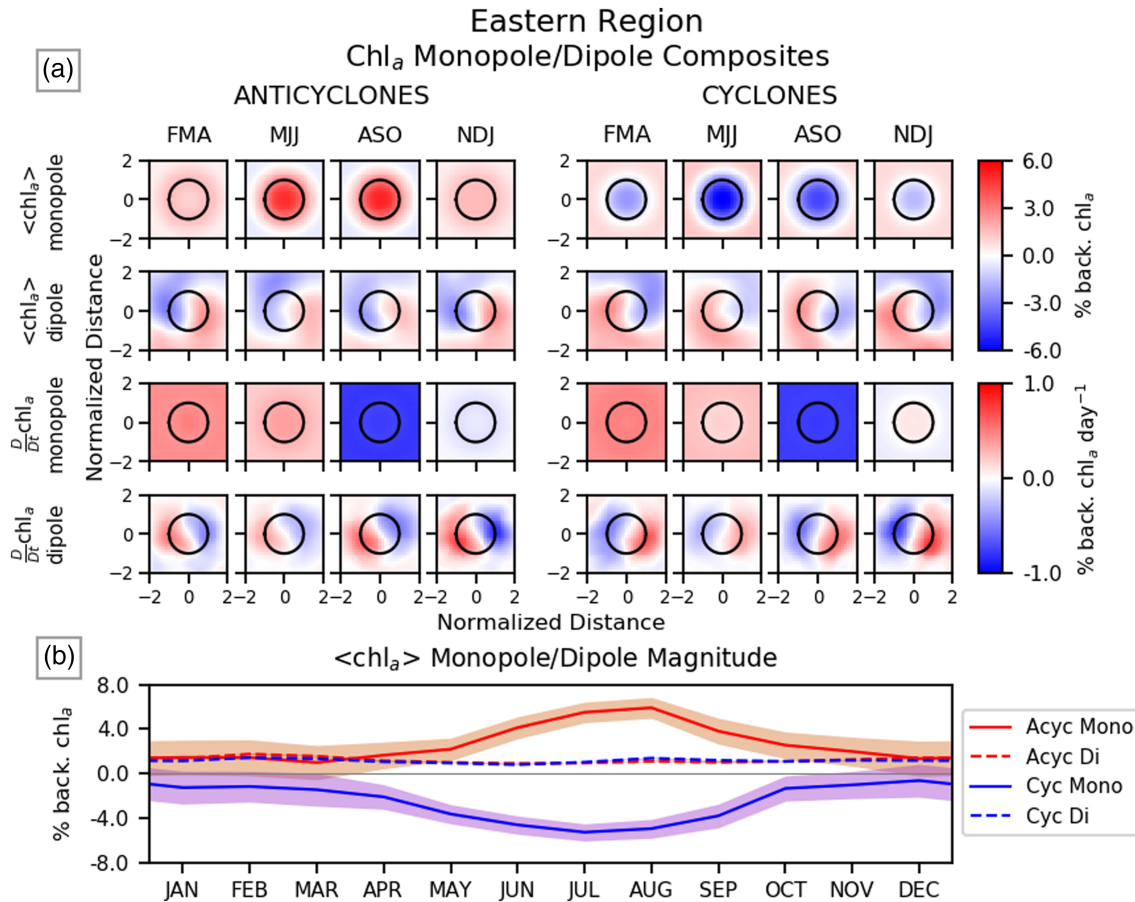


Figure 4. (a) Composites by quarterly period for the eastern South Pacific STCC (160–130°W). Anticyclones/cyclones are shown in the left/right halves of the figure, respectively. Quarterly periods are as follows: FMA = February–April, MJJ = May–July, ASO = August–October, NDJ = November–January. The first row is the monopole structure of the normalized chlorophyll anomaly, with the dipole structure shown on the second row. The color bar for these composites is the normalized chlorophyll anomaly, given as a percent of the large-scale, background chlorophyll signal. The third and fourth rows show the monopole and dipole structures, respectively, for the Lagrangian derivative $\frac{D}{Dt}(chl_a)$ of normalized chlorophyll anomalies. The color bar for these composites is a normalized chlorophyll rate of change, given as a percent of the large-scale, background chlorophyll signal per day. The black circle indicates one eddy radius from the center. (b) The relative magnitude of the monopole/dipole structure, by month, by eddy type. Anticyclones/cyclones are indicated by the red/blue lines, and monopole/dipole is indicated by the solid/dashed line. This monthly time series indicates the magnitude of the monopole and dipole structures within cyclones and anticyclones. The shaded red and blue areas indicate the 95% confidence interval for the monopole structures, using a standard t distribution, where N^* degrees of freedom are taken as the number of individual eddies used in each composite (see Figure 3).

3. Results

In the South Pacific STCC, there are distinct separations of the character of the chlorophyll response to eddies (Figure 2). This separation is expected from the inconsistent $\langle chl_a \rangle$ -ssh anomaly correlation (Figure 1b). A summary of the major results are found in Table 1. Monthly composites of chlorophyll anomalies in eddies in eastern and western region are shown in Figures 3 and 5, respectively, while monopole/dipole quartile composites of $\langle chl_a \rangle$ and $D(chl_a)/Dt$ for the eastern and western region are shown in Figures 4 and 6, respectively. Seasonal cycles of chl_a , chl'_a , and PAR_{ML} are shown in Figure 9.

In the eastern portion of the STCC, there is a consistent chlorophyll anomaly response throughout the year, with maximum anomalies occurring during the austral winter. Cyclones (anticyclones) consistently have negative (positive) chlorophyll anomalies. This is consistent with the positive $\langle chl_a \rangle$ -ssh correlation in the region. The magnitude of the chl'_a is largely in phase with the seasonal variability of the background chlorophyll (chl_a), which reaches a maximum of 0.062 mg m^{-3} in August, during the austral winter. The chlorophyll anomalies, chl'_a , can reach a maximum magnitude of 0.0031 mg m^{-3} in August and $-0.0030 \text{ mg m}^{-3}$ in July for anticyclones and cyclones, respectively. The normalized peak anomalies

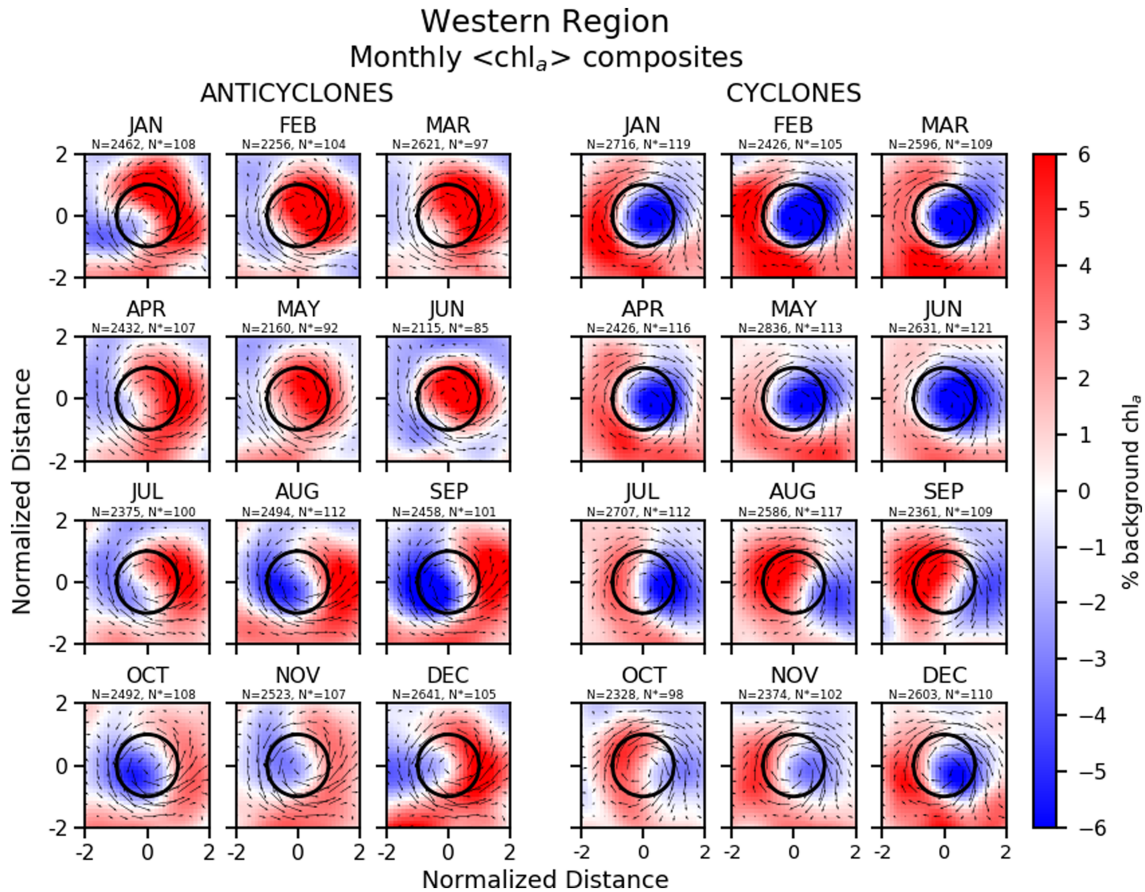


Figure 5. Composites of normalized chlorophyll anomalies in eddies in the western South Pacific STCC (165°E to 170°W) by month, as a percent of the background chlorophyll level. Anticyclones are shown by month in the left half of the figure, while cyclones are shown in the right half of the figure. The black circle indicates one eddy radius from the center. The arrows are calculated geostrophic velocity vectors, as calculated from sea surface height anomalies. The color bar indicates the normalized chlorophyll anomaly, given as a percent of the background, large-scale chlorophyll signal. Above each composite, the number of daily eddy composites used for each monthly average is given as N , while the number of individual eddies, which persist throughout the month, is given as N^* . For the purposes of conservative efforts in estimating confidence intervals, seen in Figure 4, N^* is used in an estimate of the number of degrees of freedom. For statistical characteristics of the eddies used in composites, refer to Table 1.

($\langle \text{chl}_a \rangle$) are $5.90 \pm 0.94\%$ and $-5.29 \pm 0.78\%$ of the background chlorophyll for anticyclones and cyclones, respectively (Figure 3). It should be noted that the magnitudes of these anomalies are low when compared to the tuned range of the GSM method. This highlights the advantage of the eddy-centric composites, in which the mesoscale eddy signal, even at low relative signal, can be observed.

Composites of $\langle \text{chl}_a \rangle$ and $D(\text{chl}_a)/Dt$ for the eastern STCC are shown split into a monopole/dipole structure, with the intensity of those structures varying throughout the year (Figure 4a). The composites are grouped into quarterly periods, with the peak anomaly period centered around September. The monopole/dipole structures for the eastern STCC show a consistent pattern throughout the year. Cyclones (anticyclones) have a negative (positive) chlorophyll anomaly throughout the year, which peaks to a maximum magnitude in July/August, during the austral winter. The magnitude of the dipole structure is calculated as the average of the absolute value of the $\langle \text{chl}_a \rangle$ within 1 eddy radius. The monthly average of the monopole/dipole magnitudes in cyclones and anticyclones is shown in Figure 4b. The magnitude of the dipole anomalies is similar for cyclones and anticyclones, and remains at approximately 1–2% of chl_a throughout the year. The magnitude of the dipole is of the same magnitude of the monopole during the austral summer, and is roughly half of the monopole signal during the austral winter. The $D(\text{chl}_a)/Dt$ dipole pattern strongly resembles that of the chlorophyll anomaly dipole pattern, with a reversed anomaly sign. This is indicative that the dipole pattern observed is largely due to advection of the background

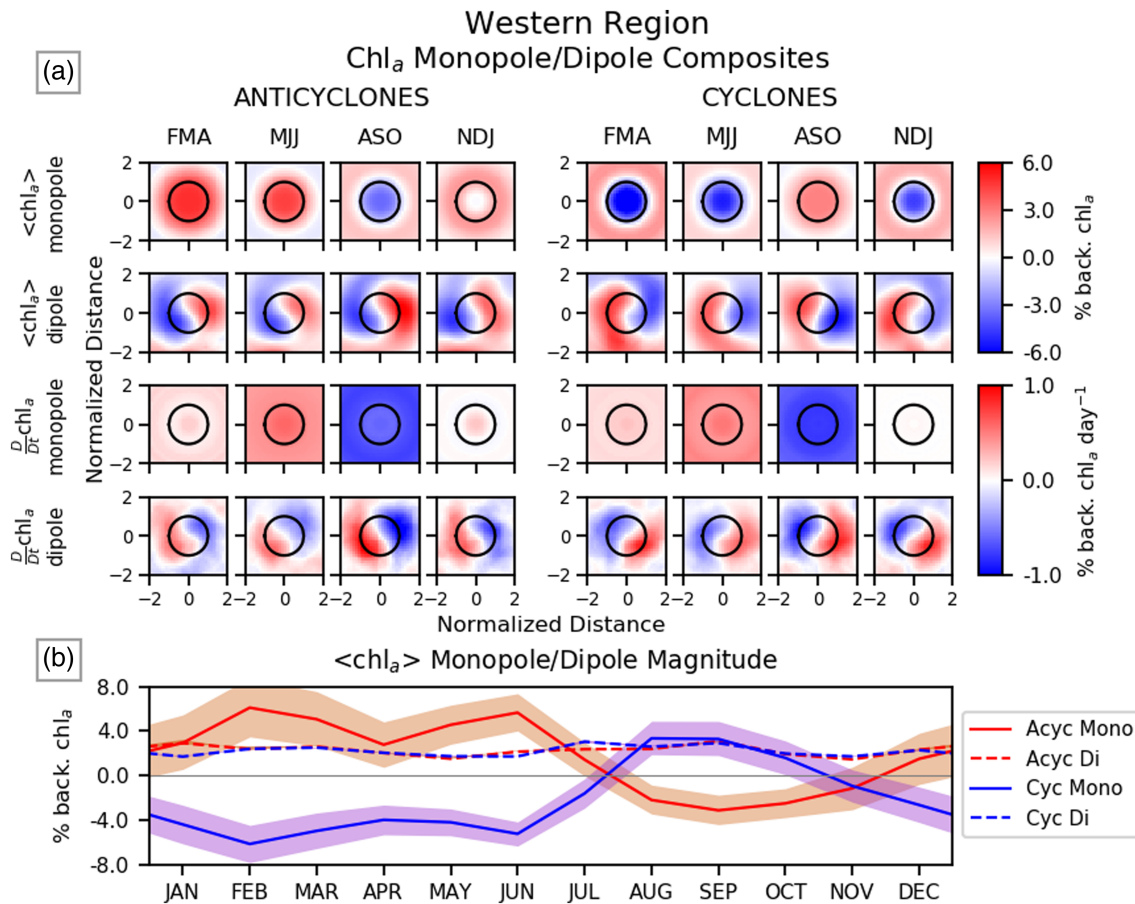


Figure 6. (a) Composites by quarterly period for the western South Pacific STCC (165°E to 170°W). Anticyclones/cyclones are shown in the left/right halves of the figure, respectively. Quarterly periods are as follows: FMA = February–April, MJJ = May–July, ASO = August–October, NDJ = November–January. The first row is the monopole structure of the normalized chlorophyll anomaly, with the dipole structure shown on the second row. The color bar for these composites is the normalized chlorophyll anomaly, given as a percent of the large-scale, background chlorophyll signal. The third and fourth rows show the monopole and dipole structures, respectively, for the Lagrangian derivative $\frac{D}{Dt}(\text{chl}_a)$ of normalized chlorophyll anomalies. The color bar for these composites is a normalized chlorophyll rate of change, given as a percent of the large-scale, background chlorophyll signal per day. The black circle indicates one eddy radius from the center. (b) The relative magnitude of the monopole/dipole structure, by month, by eddy type. Anticyclones/cyclones are indicated by the red/blue lines, and monopole/dipole is indicated by the solid/dashed line. The monthly time series indicates the magnitude of the monopole and dipole structures within cyclones and anticyclones. The shaded red and blue areas indicate the 95% confidence interval for the monopole structures, using a standard t distribution, where N^* degrees of freedom are taken as the number of individual eddies used in each composite (see Figure 3).

chlorophyll gradient. The $D(\text{chl}_a)/Dt$ monopole pattern is dominated by the background seasonal signal, with an increasing signal during the fall/winter and decreasing during the spring/fall.

In the western portion of the STCC, a very different pattern is observed. From January to June, cyclones (anticyclones) have weakly negative (positive) anomalies, whereas from July to December, cyclones (anticyclones) have positive (negative) anomalies. During the austral spring (August to October), the greatest magnitude anomalies occur, as seen in Figures 5 and 6. The chlorophyll anomaly averaged within one eddy radius ranges for cyclones is $-0.0053 \text{ mg m}^{-3}$ in March to 0.0053 mg m^{-3} in August. The range for anticyclones is 0.0055 mg m^{-3} in February to $-0.0038 \text{ mg m}^{-3}$ in September. As the background chlorophyll levels vary seasonally from 0.0780 mg m^{-3} in December to 0.1630 mg m^{-3} in August, this results in a normalized chlorophyll anomaly of $-6.17 \pm 1.67\%$ to $3.34 \pm 1.50\%$ for cyclones and $6.10 \pm 2.66\%$ to $-3.14 \pm 1.30\%$ for anticyclones. Note that the seasonal variability in the chlorophyll anomalies is out of phase with the seasonal variability of the background chlorophyll. The magnitude of the dipole structure ranges between 2.0% and 3.0% throughout the year, and is typically of the same magnitude as the monopole structure during the austral spring reversal when the dipole magnitude is greater than the monopole magnitude.

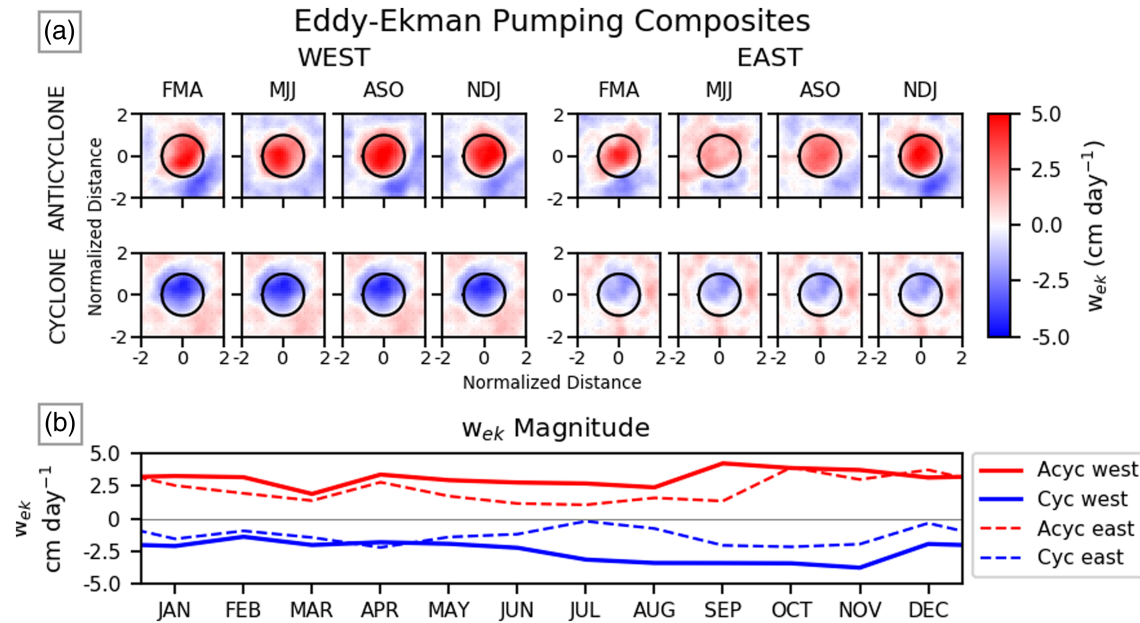


Figure 7. (a) Ekman pumping anomalies within eddies in the South Pacific STCC. Wind stress data are taken from QuikSCAT data covering the time range from January 2000 to December 2008. Composites by quarterly period are taken to match that of the chlorophyll anomalies. The left (right) side shows the composites for the western (eastern) STCC, while anticyclones (cyclones) are shown in the top (bottom) row of composites. The black circle indicates one eddy radius from the center. The color bar indicates the strength of the eddy-Ekman pumping in cm day^{-1} . (b) The monthly time series shows the magnitude of the eddy-Ekman pumping. Cyclones (anticyclones) are indicated by the blue (red) lines, while the western (eastern) composites are indicated by the solid (dashed) lines.

Using the same quartile periods as for chlorophyll anomalies, composites of the quarterly averaged eddy-Ekman pumping within eddies are constructed (Figure 7a). The magnitude of the eddy-Ekman pumping ranges between 1 and 4 cm day^{-1} for both cyclones and anticyclones, and is consistent with expectations for surface current-induced pumping. The averaged eddy-Ekman pumping is typically stronger in the western region as compared to the eastern region, particularly during the austral summer months. This weaker observed eddy-Ekman pumping in the eastern region could be caused by weaker eddy currents, as the eastern STCC typically has lower average eddy energy (Qiu et al., 2008; Travis & Qiu, 2017). This can also be seen in the average axial speed of the eddies (Table 1). There is no distinct seasonality to the pumping (Figure 7b), as well as no seasonal reversal which by itself could cause the observed seasonal reversal of the character of the chlorophyll anomalies within eddies. However, it can be conjectured that the downwelling (upwelling) in cyclones (anticyclones) generated by the eddy-Ekman pumping can be an important contributor to the nutrient supply in the eddies, and can complement the effect of the mixed layer depth anomalies. Indeed, an estimate of the relative importance can be made using a mixed layer nitrate flux budget equation.

$$\frac{\partial N}{\partial t} = -\frac{1}{H_{MLD}} (\bar{N}_{MLD} - N_B) \left(\frac{\partial H_{MLD}}{\partial t} + w_{Ek} \right) \quad (7)$$

In this equation, $\partial N/\partial t$ = the change of nitrate in the mixed layer, H_{MLD} = the mixed layer depth, \bar{N}_{MLD} = the average nitrate concentration in the mixed layer, N_B = the nitrate concentration 2 m below the base of the mixed layer, $\partial H_{MLD}/\partial t$ = the change in mixed layer depth, and w_{Ek} = the eddy-Ekman pumping velocity. From this equation, we provide an estimation of the magnitude of $\partial H_{MLD}/\partial t$ to w_{Ek} to assess their relative importance. In Figure 8, we can see that the mixed layer deepens at a maximum rate of roughly 30–50 cm day^{-1} . When compared to the average Ekman pumping magnitude of 1–4 cm day^{-1} , the entrainment of deeper nutrients from a deepening mixed layer overwhelms the Ekman pumping for most of the year.

Subsurface information relevant to the eddies in the region and the availability of light and nutrients necessary to stimulate primary production are shown in Figure 8. Throughout the STCC, the mixed layer depth of cyclones is shallower than anticyclones, with maximum mixed layer depths (MLDs) occurring in July. In the western STCC, anticyclones reach a maximum depth of approximately 80 m, while cyclones have

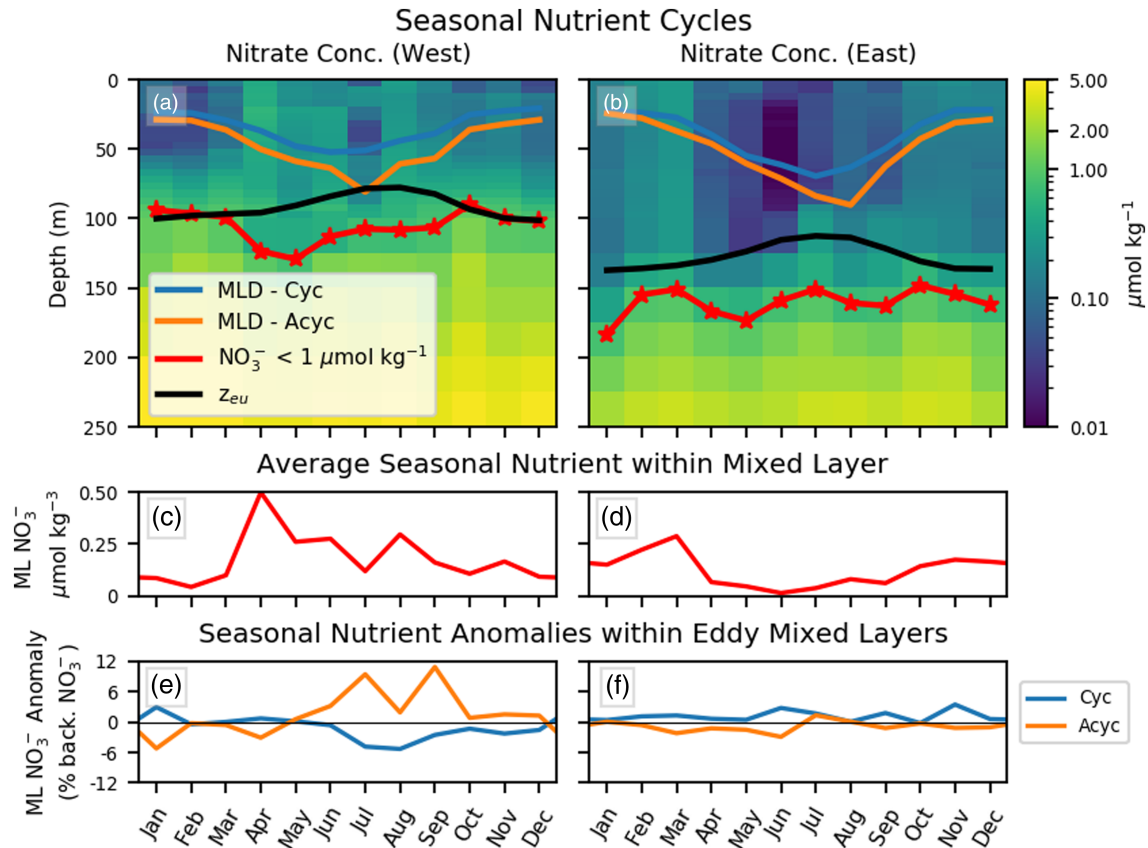


Figure 8. (a and c) The western STCC (165°E to 170°W, 22–28°S) and (b and d) the eastern STCC (160–130°W, 22–28°S). Nitrate levels (NO_3^-) in the STCC region are divided into (a) western STCC and (b) eastern STCC and averaged by month. The color bar indicates nitrate concentrations throughout the water column, given as $\mu\text{mol kg}^{-1}$ and as taken from World Ocean Atlas 2018 climatologies (WOA18). The mixed layer depth for anticyclonic and cyclonic eddies are given as the orange and blue lines, respectively. The nitracline, defined as where NO_3^- exceeds $1 \mu\text{mol kg}^{-1}$, is shown by the red line. The euphotic layer depth (z_{eu}) is shown by the black line. A monthly time series of nitrate concentration calculated within the mixed layer (c and d) and nitrate concentration anomalies within eddies (e and f) is shown. Nutrient anomalies are calculated as the percent difference of nitrate concentrations in the mixed layers within eddies from the nitrate concentrations in the mixed layers outside of eddies.

a maximum depth around 60 m. In the eastern STCC, anticyclones reach a maximum depth of 95 m and cyclones reach a maximum depth of 70 m. Between the western and eastern portions of the STCC, there are significant differences in the euphotic layer depth (z_{eu}) and in the nitracline depth. The average western euphotic layer depth is approximately 100 m, while the eastern euphotic layer depth is approximately 130 m. Lastly, the western nitracline changes from approximately 100 m in the summer to 125 m in the winter, while the eastern nitracline remains relatively constant at approximately 150 m. Note that while the choice of nitracline definition determines the observed depth, the pattern remains even with a different choice of nitracline definition. For example, at a lower definition of nitracline of 0.2 instead of $1 \mu\text{mol kg}^{-1}$, the eastern nitracline is approximately 50–75 m deeper than the western nitracline. The averaged mixed layer nitrate concentration is shown in Figures 8c and 8d, while mixed layer nitrate concentration anomalies located within eddies as a percentage of the background mixed layer nitrate concentrations are shown in Figures 8e and 8f. It should be noted that there are some unexpected fluctuations in the eastern STCC average mixed layer nitrate concentration, with a nitrate peak occurring during the summer months. This unexpected fluctuations peaks around $0.25 \mu\text{mol kg}^{-1}$, which is a relatively low concentration compared to our nitracline definition, but highlights the need for direct seasonal measurements. Current mixed layer nitrate concentrations are inferred from observed mixed layer depths with climatological nitrate levels, but more direct observations would help to quantify observed nitrate levels and nitrate fluxes. It can be seen that the deeper mixed layers of the anticyclones in the western STCC lead to a largest monthly nitrate anomaly

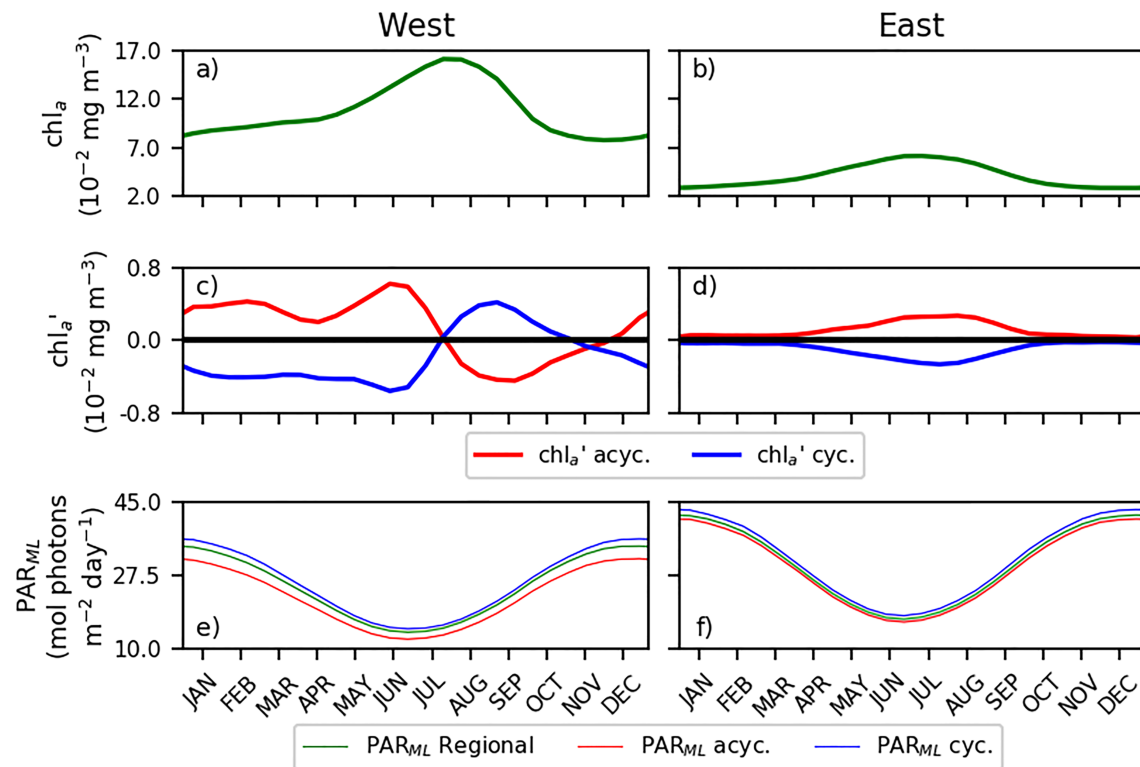


Figure 9. (a, c, and e) The western STCC (165°E to 170°W, 22–28°S), and (b, d, and f) the eastern STCC (160–130°W, 22–28°S). (a and b) Seasonal cycle of the averaged cycle of near-surface chlorophyll (chl_a). (c and d) The chl_a anomalies in cyclones and anticyclones. (e and f) Photosynthetically available radiation within the mixed layer (PAR_{ML}). The regionally averaged PAR_{ML} is given by the green line, while the PAR_{ML} within cyclones (anticyclones) is given by the blue (red) lines, respectively.

across the entire STCC region, in both cyclones and anticyclones, with peak nitrate anomalies in cyclones (anticyclones) of approximately -5% (10%) during the austral spring. In the eastern STCC, the low nitrate levels mean that there is minimal nitrate concentration anomalies throughout the year, with concentration anomaly magnitudes of $1\text{--}2\%$. The combination of changing light and nutrient availability are the most likely drivers of the changing near-surface chlorophyll response to eddies observed (Figure 2).

Figure 9 illustrates the comparative changes in background chl_a on a seasonal cycle (Figures 9a and 9b), the relative changes of anomalous chl_a on a seasonal cycle (Figures 9c and 9d), and changes in the photosynthetically available radiation within the mixed layer (PAR_{ML}) (Figures 9e and 9f). The parameters for the western STCC are shown in the left column (Figures 9a, 9c, and 9e), while the eastern STCC is shown in the right column (Figures 9b, 9d, and 9f).

For the western STCC, the background chlorophyll concentration ($\overline{chl_a}$) ranges from 0.078 mg m^{-3} in December to 0.163 mg m^{-3} in August, amounting to a 109% increase from the seasonal minimum to the seasonal maximum. PAR_{ML} in the region ranges from 13.8 to $34.5\text{ mol photons m}^{-2}\text{ day}^{-1}$. For the eastern STCC, $\overline{chl_a}$ ranges from 0.029 mg m^{-3} in December to 0.062 mg m^{-3} , creating a 114% increase. PAR_{ML} in the eastern STCC ranges from 17.0 to $42.0\text{ mol photons m}^{-2}\text{ day}^{-1}$. In both the western and eastern STCC, the seasonal changes in $\overline{chl_a}$ are inversely correlated with PAR_{ML} (western correlation = -0.77 , eastern correlation = -0.93).

4. Discussion

The spatially and temporally complicated near-surface chlorophyll signal in the presence of mesoscale eddies in the South Pacific Subtropical Countercurrent highlights the difficulty in characterizing an expected physical-biological response. Within any region, there can be significant variability throughout the year in the characterization of the environment in which eddies are found. As seen in the South Pacific STCC, even moving across a region in which eddy activity is largely the result of a single driver, namely baroclinic

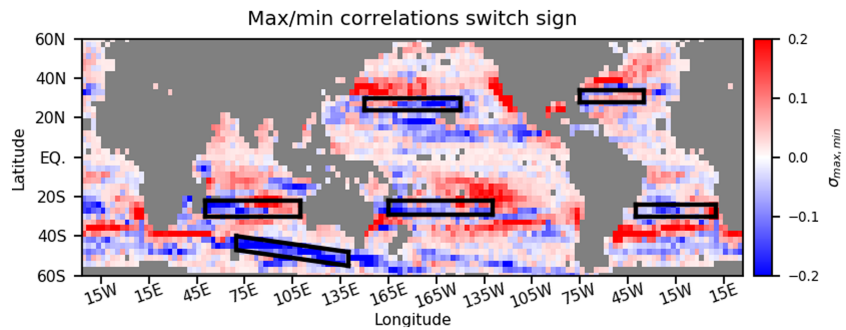


Figure 10. The multiplied maximum-minimum correlations by month ($\sigma_{\max,\min}$) are gridded into $3^\circ \times 3^\circ$ boxes. The color bar is the multiplied correlation coefficient ($\sigma_{\max,\min} = \sigma_{\max} * \sigma_{\min}$), where σ is the correlation coefficient for any given month. Regions with a seasonally consistent $\langle \text{chl}_a \rangle$ -ssh anomaly correlation are shown in red. Regions with a seasonal switch of the sign of the correlation (positive and negative correlations throughout the year) are shown in blue and are areas of a possible reversal of the sign of the chlorophyll anomaly response to eddies. Possible regions of interest are highlighted by the black boxes.

instabilities (Travis & Qiu, 2017), there can be a shift in the character of the response to the same eddies. Globally, this creates the possibility that there are areas in which this seasonally reversing biological response have been overlooked.

To identify regions which could exhibit a seasonal reversal of the type of chlorophyll response to the presence of eddies, a $\langle \text{chl}_a \rangle$ -ssh anomaly correlation is calculated for each month ($\sigma(\text{month})$). From these correlations, the maximum and minimum correlation among each of the 12 months found at a grid point are multiplied together.

$$\sigma_{\max,\min} = \max(\sigma(\text{month})) * \min(\sigma(\text{month})) \quad (8)$$

This combined correlation will always be positive if the maximum and minimum correlations among the months are the same sign (i.e., always a positive or always a negative correlation). The combined correlation will only be negative if the maximum and minimum correlations among the months are of opposite sign. In this case, SSH and chl_a anomalies are positively correlated for part of the year and negatively correlated for part of the year. In Figure 10, $\sigma_{\max*\min}$ is binned into $3^\circ \times 3^\circ$ grids.

A number of regions with negative combined correlations are identified, as seen in Figure 10, and are indicative of seasonal reversal of the chlorophyll response to eddies. Some of the identified regions are the South Pacific STCC, the South Indian STCC, the ACC, the North Pacific STCC, the North Atlantic STCC, and the South Atlantic STCC, and are highlighted by the black boxes in Figure 10. A common feature among these currents, with the exception of the ACC, is that they lie near the boundary between typically highly oligotrophic regions and relatively more productive waters. Recent work in the ACC (Dawson et al., 2018; Song et al., 2018) also observed a seasonal variation in the type of chlorophyll anomaly response to eddies, emphasizing the importance of changing mixed layer depths and nutrient availability in determining the expected physical-biological response to eddies.

Seasonal cycles of chlorophyll anomalies within mesoscale eddies for a number of the above listed regions are shown in Figure 11. From the figure, it can be seen that magnitude of the anomalies and the timing and duration of the seasonal reversal is highly variable among the regions. This is indicative of the large number of factors that could be affecting the physical-biological responses and driving the seasonal reversal. For instance, we see the seasonal reversal of the anomalous chlorophyll signal in the winter/spring in the South Pacific STCC (Figure 2), whereas in the South Indian STCC (Figures 11a and 11b), the reversal occurs during the summer. In the South Indian STCC, it has been observed that an anomalous summer bloom to the east of Madagascar is associated with a change in phytoplankton community structure, moving to nitrogen-fixing phytoplankton (Poulton et al., 2009), and it has been explored as to whether the bloom is fertilized by iron from Madagascar (Srokosz et al., 2015). It is unknown how this shift in community structure would manifest within the eddying flows, and warrants further investigation. This region is also demonstrative of the need to look more deeply into each of the regions highlighted in Figures 10 and 11.

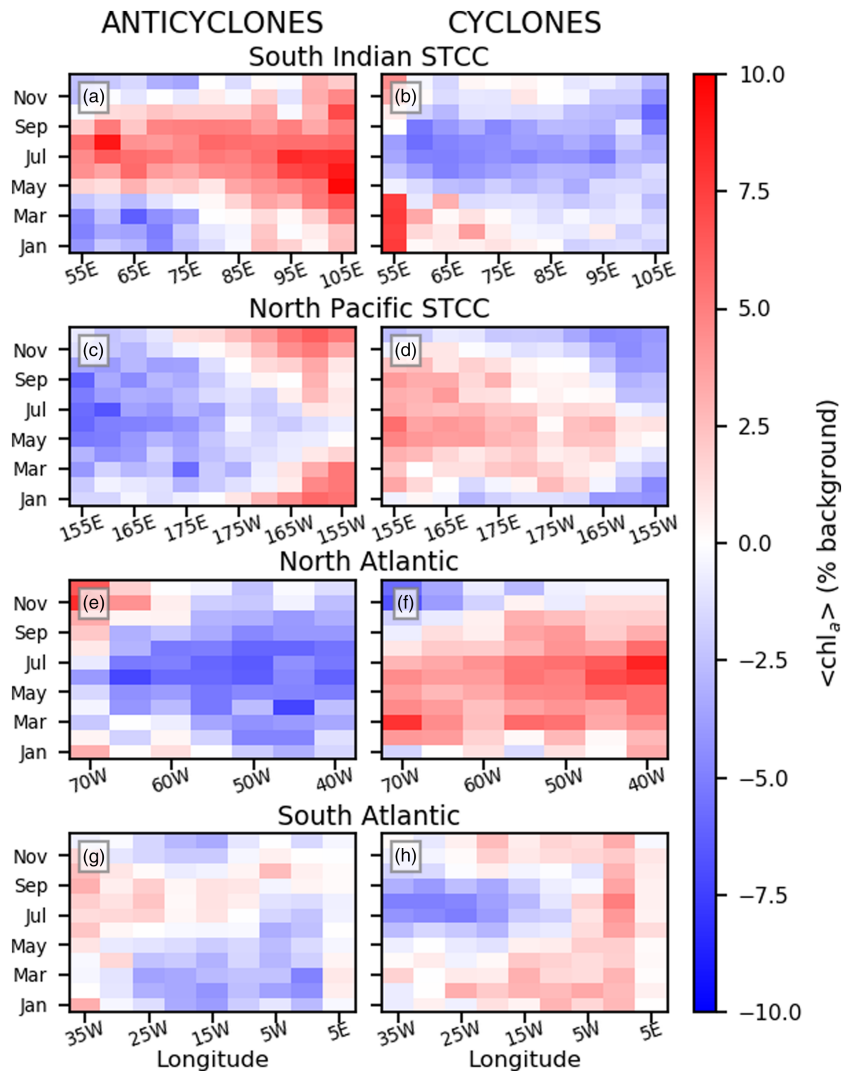


Figure 11. Hovmueller x - t diagrams of normalized chlorophyll anomalies ($\langle \text{chl}_a \rangle$) by month for the regions highlighted in Figure 10 by the black boxes. Hovmueller diagrams for the South Pacific STCC can be found in Figure 2, while the ACC diagrams are not included. The left column shows the anomalies for anticyclones, and the right column shows the anomalies for cyclones. The color bar is the normalized chlorophyll anomaly, given as a percent of the large-scale, background chlorophyll signal. (a and b) South Indian STCC (50–110°E, 22–30°S). (c and d) North Pacific STCC (150°E to 150°W, 24°N to 30°S). (e and f) North Atlantic STCC (75–35°W, 28–34°N). (g and h) South Atlantic STCC (40°W to 10°E, 24–30°S).

5. Summary

By isolating near-surface chlorophyll at the mesoscale length scales, the physical-biological effect of eddies can be seen from satellite data. In the South Pacific STCC, this signal is found to be highly spatially and temporally complicated. In the east, chl'_a in mesoscale eddies exhibit a response consistent with a nutrient-limited regime throughout the year. In the west, the chlorophyll signal indicates a seasonally inconsistent response, with alternating positive/negative anomalies with the changing seasons. Cyclones (anticyclones) exhibit a negative (positive) response signal during the summer months and a positive (negative) signal during the winter months. This pattern is consistent with a nutrient-limited regime during the summer months and a light-limited regime during the winter months.

Examining seasonal trends in climatological nutrient availability across the STCC gives evidence to support these observed patterns. In the eastern STCC, the deep nitracline exceeds 150 m throughout the whole year, with the euphotic zone extending down to 120–130 m throughout the year. As the seasonally varying mixed layer ranges from roughly 30 m for all eddies in the summer to 100 m for anticyclones and 80 m for cyclones,

it is observed that the mixed layer depth is consistently shallower than the euphotic zone and the nitracline. In this area, the chlorophyll anomaly patterns are consistent with the expected response for a region where nutrient availability within the mixed layer is the limiting factor.

A very different pattern emerges in the western STCC. The nitracline is shallower, with typical depths between 90–120 m and a maximum (minimum) during the winter (summer). This is also approximately the range of the euphotic zone, which has a maximum during the summer and a minimum during the winter. During the summer months, the mixed layer depth is at a minimum, and typically 20–40 m deep. During this time, there is low nitrate concentration within the mixed layer for both eddy types. In the winter, the deeper mixed layers are able to reach down below the euphotic zone and access the deeper nutrient pool. In this case, higher nutrient availability and deeper mixing below the euphotic zone provide the conditions to shift the character of the environment to one consistent with a light-limited regime for chlorophyll anomalies. This is also supported by the lower overall PAR_{ML} found throughout the western STCC as compared to the eastern STCC, as well as lower PAR_{ML} within anticyclones as compared to cyclones.

Taking into account all of these patterns, the changing near-surface chlorophyll response in the presence of eddies in the western STCC can be explained. If the character of the environment of the western STCC were the same as that of the eastern STCC, we would expect to see chlorophyll anomaly patterns consistent with nutrient limitation in the mixed layer, that is, positive anomalies in anticyclones and negative anomalies in cyclones. Light limitation would produce a reversed pattern, that is, negative anomalies in anticyclones and positive anomalies in cyclones. The deeper mixed layers of anticyclones would decrease average light levels, leading to decreased productivity, and subsequently, lower chlorophyll levels, while the opposite would happen in cyclones. In the western STCC, the observed chlorophyll anomaly patterns in the region are consistent with nutrient limitation throughout the summer, when shallow mixed layers keep the deep nutrient supply isolated from the surface. During the winter, however, the mixed layer deepens, increasing the nitrate concentrations throughout the mixed layer. The mixed layer deepens beneath the euphotic layer, and it is inferred that the regime switches to being light-limited. This switch from a nutrient-limited regime to a light-limited regime causes the reversal in the anomalous chlorophyll response found within eddies in the region. This is contrasted with the eastern STCC, where the region is inferred to be nutrient-limited throughout the whole year. The nitracline in the eastern STCC is about 25–50 m deeper than the western STCC, and remains isolated from the surface for the whole year. Because the region remains in a nutrient-limited regime, the character of the anomalous response is consistent throughout the year.

There are a number of effects and mechanisms that have not been accounted for in this work, such as the changes in the deep chlorophyll maximum which may not be observable by satellites (McGillicuddy et al., 2007), submesoscale dynamics (Zhang et al., 2019), and predation mechanisms, to name a few. For instance, top-down dynamics, such as predator grazing, would not be distinguishable in the chlorophyll anomaly signals, and would complicate efforts to assess the potential for new production. Despite these limitations, this work highlights the need for taking into account all dynamics, including regionally and seasonally changing dynamics, when characterizing the physical-biological response to the presence of mesoscale eddies. Observational studies utilizing subsurface data, including data for Bio-Argo floats, such as those done by Dufois et al. (2017) and by Mignot et al. (2014), will be increasingly important in characterizing the dynamics within eddies in a region. The characterization of the mesoscale physical-biological response will require a careful understanding of the state of the ocean and all of the limiting factors involved, and increasing observational capabilities will improve our understanding of these factors and the dynamical processes which affect them.

Acknowledgments

The authors would like to acknowledge constructive feedback from two reviewers, which led to improvements of this paper. The authors acknowledge funding support from NASA Grant NNX17AH33G. The Argo data used in this study were collected and made freely available by the International Argo Program and the national programs that contribute to it. The Argo data was accessed (via <https://www.usgoda.gov/argo/argo.html>). GlobColour data (<http://globcolour.info>) used in this study have been developed, validated, and distributed by ACRI-ST, France. The altimeter products were produced by Ssalto/Duacs and distributed by Aviso+, with support from CNES (<https://www.aviso.altimetry.fr/duacs/>). QuikScat data are produced by Remote Sensing Systems and sponsored by the NASA Ocean Vector Winds Science Team. Data are available online (at www.remss.com). The gridded, daily data product of QuikSCAT V3 wind stress is provided by Ifremer. These data were obtained from the Centre de Recherche et d'Exploitation Satellitaire (CERSAT), at IFREMER, Plouzané (France).

References

- Bailleul, F., Cotté, C., & Guinet, C. (2010). Mesoscale eddies as foraging area of a deep-diving predator, the southern elephant seal. *Marine Ecology Progress Series*, 408, 251–264. <https://doi.org/10.3354/meps08560>
- Behrenfeld, M. J., Boss, E., Siegel, D. A., & Shea, D. M. (2005). Carbon-based ocean productivity and phytoplankton physiology from space. *Global Biogeochemical Cycles*, 19, GB1006. <https://doi.org/10.1029/2004GB002299>
- Bender, M. L., & Jonsson, B. (2016). Is seasonal net community production in the South Pacific Subtropical Gyre anomalously low? *Geophysical Research Letters*, 43, 9757–9763. <https://doi.org/10.1002/2016GL070220>
- Campbell, J. W. (1995). The lognormal distribution as a model for bio-optical variability in the sea. *Journal of Geophysical Research*, 100(C7), 13237. <https://doi.org/10.1029/95JC00458>
- Chelton, D. B., Gaube, P., Schlax, M. G., Early, J. J., & Samelson, R. M. (2011). The influence of nonlinear mesoscale eddies on near-surface oceanic chlorophyll. *Science*, 334(6054), 328–332. <https://doi.org/10.1126/science.1208897>
- Condie, S., & Condie, R. (2016). Retention of plankton within ocean eddies. *Global Ecology and Biogeography*, 25(10), 1264–1277. <https://doi.org/10.1111/geb.12485>

- Dawson, H. R. S., Strutton, P. G., & Gaube, P. (2018). The unusual surface chlorophyll signatures of Southern Ocean eddies. *Journal of Geophysical Research: Oceans*, *123*, 6053–6069. <https://doi.org/10.1029/2017JC013628>
- Dong, C., McWilliams, J. C., Liu, Y., & Chen, D. (2014). Global heat and salt transports by eddy movement. *Nature Communications*, *5*, 3294. <https://doi.org/10.1038/ncomms4294>
- Dufois, F., Hardman-Mountford, N. J., Fernandes, M., Wojtasiewicz, B., Shenoy, D., Slawinski, D., et al. (2017). Observational insights into chlorophyll distributions of subtropical South Indian Ocean eddies. *Geophysical Research Letters*, *44*, 3255–3264. <https://doi.org/10.1002/2016GL072371>
- Dufois, F., Hardman-Mountford, N. J., Greenwood, J., Richardson, A. J., Feng, M., Herbette, S., & Matear, R. (2014). Impact of eddies on surface chlorophyll in the South Indian Ocean. *Journal of Geophysical Research: Oceans*, *119*, 8061–8077. <https://doi.org/10.1002/2014JC010164>
- Dufois, F., Hardman-mountford, N. J., Greenwood, J., Richardson, A. J., Feng, M., & Matear, R. J. (2016). Anticyclonic eddies are more productive than cyclonic eddies in subtropical gyres because of winter mixing. *Science*, *2*, e1600282. <https://doi.org/10.1126/sciadv.1600282>
- Dufour, C. O., Griffies, S. M., de Souza, G. F., Frenger, I., Morrison, A. K., Palter, J. B., et al. (2015). Role of mesoscale eddies in cross-frontal transport of heat and biogeochemical tracers in the Southern Ocean. *Journal of Physical Oceanography*, *45*, 3057–3081. <https://doi.org/10.1175/JPO-D-14-0240.1>
- Frenger, I., Münnich, M., & Gruber, N. (2018). Imprint of Southern Ocean mesoscale eddies on chlorophyll. *Biogeosciences*, *15*(15), 4781–4798. <https://doi.org/10.5194/bg-15-4781-2018>
- Garcia, H. E., Weathers, K. W., Paver, C. R., Smolyar, I., Boyer, T. P., Locarnini, R. A., et al. (2019). World Ocean atlas 2018. Vol. 4: Dissolved inorganic nutrients (phosphate, nitrate and nitrate+nitrite, silicate). *NOAA Atlas NESDIS 84*, 4, 35.
- Gaube, P., Chelton, D. B., Samelson, R. M., Schlax, M. G., & O'Neill, L. W. (2015). Satellite observations of mesoscale eddy-induced Ekman pumping. *Journal of Physical Oceanography*, *45*(1), 104–132. <https://doi.org/10.1175/JPO-D-14-0032.1>
- Gaube, P., Chelton, D. B., Strutton, P. G., & Behrenfeld, M. J. (2013). Satellite observations of chlorophyll, phytoplankton biomass, and Ekman pumping in nonlinear mesoscale eddies. *Journal of Geophysical Research: Oceans*, *118*, 6349–6370. <https://doi.org/10.1002/2013JC009027>
- Gaube, P., McGillicuddy, D. J., Chelton, D. B., Behrenfeld, M. J., & Strutton, P. G. (2014). Regional variations in the influence of mesoscale eddies on near-surface chlorophyll. *Journal of Geophysical Research: Oceans*, *119*, 8195–8220. <https://doi.org/10.1002/2014JC010111>
- Gaube, P., McGillicuddy, D. J., & Moulin, A. J. (2019). Mesoscale eddies modulate mixed layer depth globally. *Geophysical Research Letters*, *46*, 1505–1512. <https://doi.org/10.1029/2018GL080006>
- Godø, O. R., Samuelsen, A., Macaulay, G. J., Patel, R., Hjøllø, S. S., Kaartvedt, S., & Johannessen, J. A. (2012). Mesoscale eddies are oases for higher trophic marine life. *PLoS One*, *7*(1), 1–9. <https://doi.org/10.1371/journal.pone.0030161>
- Guidi, L., Calil, P. H. R., Duhamel, S., Björkman, K. M., Doney, S. C., Jackson, G. A., et al. (2012). Does eddy-eddy interaction control surface phytoplankton distribution and carbon export in the North Pacific Subtropical Gyre? *Journal of Geophysical Research*, *117*, G02024. <https://doi.org/10.1029/2012JG001984>
- He, Q., Zhan, H., Cai, S., & Li, Z. (2016). Eddy effects on surface chlorophyll in the northern South China Sea: Mechanism investigation and temporal variability analysis. *Deep-Sea Research Part I: Oceanographic Research Papers*, *112*, 25–36. <https://doi.org/10.1016/j.dsr.2016.03.004>
- He, Q., Zhan, H., Cai, S., & Zha, G. (2016). On the asymmetry of eddy-induced surface chlorophyll anomalies in the southeastern Pacific: The role of eddy-Ekman pumping. *Progress in Oceanography*, *141*, 202–211. <https://doi.org/10.1016/j.pocean.2015.12.012>
- Holte, J., Talley, L. D., Gilson, J., & Roemmich, D. (2017). An Argo mixed layer climatology and database. *Geophysical Research Letters*, *44*, 5618–5626. <https://doi.org/10.1002/2017GL073426>
- Huang, J., & Xu, F. (2018). Observational evidence of subsurface chlorophyll response to mesoscale eddies in the North Pacific. *Geophysical Research Letters*, *45*, 8462–8470. <https://doi.org/10.1029/2018GL078408>
- Klein, P., & Lapeyre, G. (2009). The oceanic vertical pump induced by mesoscale and submesoscale turbulence. *Annual Review of Marine Science*, *1*(1), 351–375. <https://doi.org/10.1146/annurev.marine.010908.163704>
- Lavelle, J. W., & Mohn, C. (2010). Motion, commotion, and biophysical connections at deep ocean seamounts. *Oceanography*, *23*(01), 90–103. <https://doi.org/10.5670/oceanog.2010.64>
- Maritorena, S., Siegel, D. A., & Peterson, A. R. (2002). Optimization of a semianalytical ocean color model for global-scale applications. *Applied Optics*, *41*(15), 2705. <https://doi.org/10.1364/AO.41.002705>
- Martin, A. P., & Richards, K. J. (2001). Mechanisms for vertical nutrient transport within a North Atlantic mesoscale eddy. *Deep-Sea Research Part II: Topical Studies in Oceanography*, *48*(4-5), 757–773. [https://doi.org/10.1016/S0967-0645\(00\)00096-5](https://doi.org/10.1016/S0967-0645(00)00096-5)
- McClain, C. R., Signorini, S. R., & Christian, J. R. (2004). Subtropical gyre variability observed by ocean-color satellites. *Deep Sea Research Part II: Topical Studies in Oceanography*, *51*(1-3), 281–301. <https://doi.org/10.1016/j.dsr2.2003.08.002>
- McGillicuddy, D. J. (2016). Mechanisms of physical-biological-biogeochemical interaction at the oceanic mesoscale. *Annual Review of Marine Science*, *8*(1), 125–159. <https://doi.org/10.1146/annurev-marine-010814-015606>
- McGillicuddy, D. J., Anderson, L. A., Bates, N. R., Bibby, T., Buesseler, K. O., Carlson, C. A., et al. (2007). Eddy/wind interactions stimulate extraordinary mid-ocean plankton blooms. *Science*, *316*(5827), 1021–1026. <https://doi.org/10.1126/science.1136256>
- Mignot, A., Claustre, H., Uitz, J., Poteau, A., D'Ortenzio, F., & Xing, X. (2014). Understanding the seasonal dynamics of phytoplankton biomass and the deep chlorophyll maximum in oligotrophic environments: A Bio-Argo float investigation. *Global Biogeochemical Cycles*, *28*, 856–876. <https://doi.org/10.1002/2013GB004781>
- Morato, T., Bulman, C., & Pitcher, T. J. (2009). Modelled effects of primary and secondary production enhancement by seamounts on local fish stocks. *Deep-Sea Research Part II: Topical Studies in Oceanography*, *56*(25), 2713–2719. <https://doi.org/10.1016/j.dsr2.2008.12.029>
- Morel, A., Claustre, H., & Gentili, B. (2010). The most oligotrophic subtropical zones of the global ocean: Similarities and differences in terms of chlorophyll and yellow substance. *Biogeosciences*, *7*(10), 3139–3151. <https://doi.org/10.5194/bg-7-3139-2010>
- Morel, A., Huot, Y., Gentili, B., Werdell, P. J., Hooker, S. B., & Franz, B. A. (2007). Examining the consistency of products derived from various ocean color sensors in open ocean (Case 1) waters in the perspective of a multi-sensor approach. *Remote Sensing of Environment*, *111*(1), 69–88. <https://doi.org/10.1016/j.rse.2007.03.012>
- Poulton, A. J., Stinchcombe, M. C., & Quartly, G. D. (2009). High numbers of Trichodesmium and diazotrophic diatoms in the southwest Indian Ocean. *Geophysical Research Letters*, *36*, L15610. <https://doi.org/10.1029/2009GL039719>
- Qiu, B., Scott, R. B., & Chen, S. (2008). Length scales of eddy generation and nonlinear evolution of the seasonally modulated South Pacific Subtropical Countercurrent. *Journal of Physical Oceanography*, *38*(7), 1515–1528. <https://doi.org/10.1175/2007JPO3856.1>

- Rieck, J. K., Böning, C. W., & Greatbatch, R. J. (2018). Decadal variability of eddy kinetic energy in the South Pacific Subtropical Countercurrent in an ocean general circulation model. *Journal of Physical Oceanography*, *48*(4), 757–771. <https://doi.org/10.1175/JPO-D-17-0173.1>
- Schlax, M. G., & Chelton, D. B. (2016). The “growing method” of eddy identification and tracking in two and three dimensions. Oregon, July 8, 2016: College of Earth, Ocean and Atmospheric Sciences, Oregon State University, Corvallis.
- Shulzitski, K., Sponaugle, S., Hauff, M., Walter, K. D., & Cowen, R. K. (2016). Encounter with mesoscale eddies enhances survival to settlement in larval coral reef fishes. *Proceedings of the National Academy of Sciences*, *113*(25), 6928–6933. <https://doi.org/10.1073/pnas.1601606113>
- Song, H., Long, M. C., Gaube, P., Frenger, I., Marshall, J., & McGillicuddy, D. J. (2018). Seasonal variation in the correlation between anomalies of sea level and chlorophyll in the Antarctic Circumpolar Current. *Geophysical Research Letters*, *45*, 5011–5019. <https://doi.org/10.1029/2017GL076246>
- Srokosz, M. A., Robinson, J., McGrain, H., Popova, E. E., & Yool, A. (2015). Could the Madagascar bloom be fertilized by Madagascan iron? *Journal of Geophysical Research: Oceans*, *120*, 5790–5803. <https://doi.org/10.1002/2015JC011075>
- Travis, S., & Qiu, B. (2017). Decadal variability in the South Pacific Subtropical Countercurrent and regional mesoscale eddy activity. *Journal of Physical Oceanography*, *47*(3), 499–512.
- von Storch, H., & Zwiers, F. W. (1999). *Statistical analysis in climate research*. Cambridge: Cambridge University Press. <https://doi.org/10.1017/CBO978051161233>
- Zhang, Z., Qiu, B., Klein, P., & Travis, S. (2019). The influence of geostrophic strain on oceanic ageostrophic motion and surface chlorophyll. *Nature Communications*, *10*(2838), 1–11. <https://doi.org/10.1038/s41467-019-10883-w>
- Zhang, Z., Wang, W., & Qiu, B. B. (2014). Oceanic mass transport by mesoscale eddies. *Science*, *345*(6194), 322–324. <https://doi.org/10.1126/science.1252418>